JOURNAL OF MATERIALS SCIENCE 28 (1993) 4047–4052

Acoustic emission analysis and small-angle X-ray scattering from microcracks during deformation of ETFE composites

R. KRAUS, A. PAYER, W. WILKE
Abteilung Experimentelle Physik, Universität Ulm, Albert-Einstein-Allee 11, 7900 Ulm, Germany

During the deformation of an unfilled matrix of ethylene–tetrafluoroethylene (ETFE), microcracking was observed by small-angle X-ray scattering (SAXS), although it does not cause significant acoustic emission because the released energy is too small to be detected (size of microcracks ≪ size of fibres). Fibres induce local stress maxima and increase the formation of microcracks. Fibre delamination processes were monitored by acoustic emission analysis. The use of coupling agents improves the fibre–matrix adhesion and increases the mechanical yield stress and decreases delamination processes. A simple model for estimating the energy released by fibre delamination processes was suggested. The predicted difference in peak amplitude between the two extreme processes agrees well with the results of the experiments. The characteristic values of the peak amplitude distributions, however, do not show any significant dependence on fibre coating or testing temperature. Further investigations by SAXS and acoustic emission analysis, especially at low strain, will be necessary to obtain more detailed information about the initial formation of microcracks and fibre delamination.

1. Introduction

Acoustic emission analysis is widely used for monitoring fracture processes in long-fibre and laminate composites. Wolters [1] described the basic principles for the application of acoustic emission analysis to short-fibre reinforced thermoplastics. The objective of the present work was the characterization of failure mechanisms occurring during tensile testing of ethylene–tetrafluoroethylene (ETFE) composites reinforced by short glass fibres. Small-angle X-ray scattering (SAXS) measurements show scattering from microcracks both in the composite and in the pure matrix material. Therefore acoustic emission analysis was used to obtain additional information about the failure mechanisms in these composites.

2. Theory

2.1. Failure processes in short-fibre composites

Three basic failure modes caused by uniaxial deformation of short fibre composites are as follows:

1. Matrix cracking. This occurs both in the pure polymer matrix and in fibre-reinforced composites by the formation of

(a) submicrocracks,
(b) crazes perpendicular to the strain direction, and
(c) interfibrillar microcracks parallel to the strain direction;

2. Failure of the matrix–fibre interface. This occurs because of

(a) stress applied normal to the fibre surface (debonding) and
(b) shear stress leading to fibre pull-out.

Depending on the strength of the fibre–matrix interface, the matrix slips off the fibres (bad contact, adhesive failure) or breaks near the interface (good contact, cohesive failure).

3. Fibre breakage. If the stress applied to the fibres becomes greater than their strength, fibres will break.

2.2. The amplitude distribution function

The stress wave propagation in the specimen is very difficult to describe [2] since the wavelength is comparable to the specimen size. Experiments using model composites with single fibres show that the peak amplitude measured from an acoustic emission event is proportional to the energy released by the underlying failure process [1]. Failure mechanisms with different energy values should be characterized by their peak amplitude values. Lorenzo and Hahn [3] performed a computer simulation for fibre breakage in a model composite. The resulting (cumulative) amplitude distribution was modelled by a Weibull distribution function with two parameters b and c in the equation

$$\Phi(A) = 1 - \exp\left[1 - \left(\frac{A}{b}\right)^{-c}\right] \quad (1)$$

0022–2461

There is generally more than one failure mode during the composite deformation process. Wu *et al.* [4] proposed a linear combination of individual distributions to describe the amplitude spectrum of the entire process.

This distribution function requires the measured amplitude distribution data to be normalized to unity. Another problem is the lower amplitude limit, which results from the fixed threshold level. Therefore and for easier interpretation we used the corresponding distributive function:

$$\varphi(A) = -\frac{d\Phi(A)}{dA} \quad (2)$$

$$\varphi_i(A) = a_i\left(\frac{A}{b_i}\right)^{-(c_i+1)} \exp\left[-\left(\frac{A}{b_i}\right)^{-c_i}\right] \quad (3)$$

$$\varphi = \sum_{i=1}^{n} \varphi_i(a_i, b_i, c_i) \quad (4)$$

where a = normalization factor, b = most frequent peak amplitude value and c = width of distribution. Now the linear combination is given by adding the individual distributions.

3. Experimental procedure

3.1. Materials and specimens

The ETFE matrix was a copolymer of ethylene (38.5%) and tetrafluoroethylene (61.5%) with a low fraction (0.4%) of perfluoropropylvinylether (PPVE) produced by Hoechst.

The fibres were glass fibres (E glass) with an average diameter of 10 μm and an average length of $\bar{L}$ = 60 μm. One fraction of the fibres was treated with the coupling agent LZ44 (neopentyl(diallyl)oxytri (N-ethylenediamino)ethylzirconate) to improve the fibre–matrix interface.

The specimens were prepared by melting the mixture of matrix and a weight fraction of 10% of fibres under pressure (p = 25 bar) at a temperature of 295 °C, followed by cooling to room temperature (cooling rate approximately 3 K min^{-1}).

The influence of the coupling agent on the fibre–matrix interface was studied by breaking composites at low temperature ($T \simeq -190$ °C, liquid nitrogen) and analysing the fracture surface by scanning electron microscopy. Electron micrographs (Figs 1 and 2) show that in the composite made of fibres without coupling agent, the matrix is removed from the fibres. In the composite made of the fibres treated with coupling agent LZ44 most of the fibres are covered with polymer matrix. This indicates that the fibre–matrix interface is improved by the coupling agent.

3.2. Small-angle X-ray scattering

The SAXS experiments were carried out with samples of the pure matrix and composites with 20% by volume fibre content. The coupling agent was Lica 97 (neopentyl(diallyl)oxytri(m-amino)phenyltitanate).

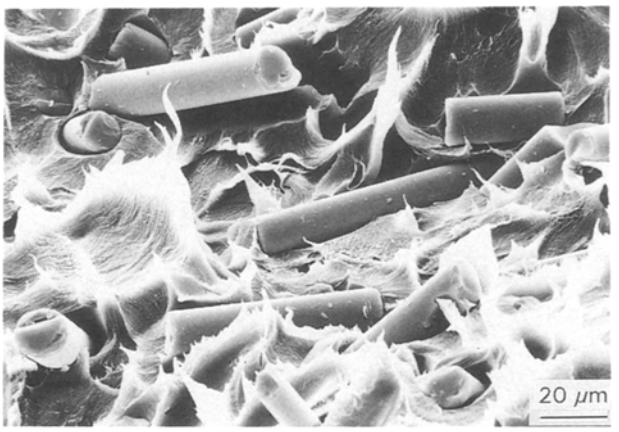

Figure 1 ETFE with fibres not treated with coupling agent.

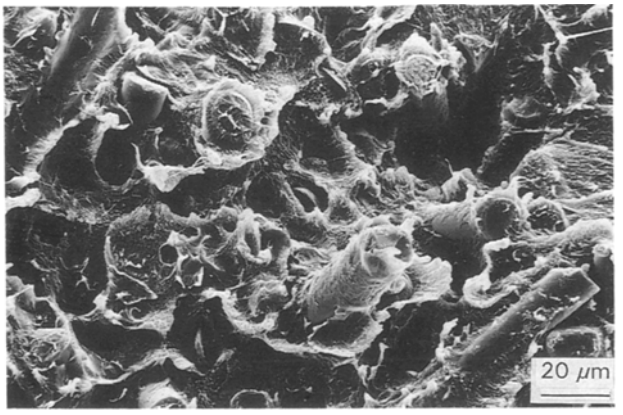

Figure 2 ETFE with fibres treated with LZ44.

3.3. Test methods

Tensile tests were performed on a Zwick testing machine at a constant speed of 5 mm min^{-1}. Acoustic emissions were monitored on an AET Model 5500 system. The AET 5500 was set up in linear test mode with two transducers attached to the specimen by spring clamps. The transducers were standard AET AC375L with a resonant frequency of 375 kHz and a sensitivity better than −70 dB referred to 1 V(μbar)$^{-1}$. The detected signals were passed through a bandpass filter FL-25 with a flat frequency response between 250 and 500 kHz. Then they were preamplified in an AET Model 140B preamplifier with a total gain of 40 dB and a flat frequency response between 1 kHz and 2 MHz. Final amplification was performed by the AET Signal Processing Unit with 39 dB. The preset parameters are given in Table I.

The acoustic emission data were analysed by custom-made software to correct the amplitude values for attenuation in the specimen. Especially in thermoplastic composites the acoustic emission signals are strongly attenuated when they are transmitted through the specimen before they reach the sensor. Wolters [1] suggested a method to correct the amplitude values. The origin of an acoustic emission event can be localized when the event is detected by two sensors. With a given attenuation value d in the specimen it is possible to calculate the original peak ampli-

TABLE I AE preset parameters

Parameter	Preset value
Preamplifier gain (dB)	40
Amplifier gain (dB)	39
Threshold voltage, V (fixed)	0.5
Event duration clock (ns)	1000
Longest event (μs)	3839
Dead time (μs)	256
Rise time clock (ns)	250
Distance locator clock (ns)	250
Acceptance criteria	
Ring down counts	$3 < N < 4095$
Event duration (μs)	$2 < T < 3839$

tude A of the event at the place where it happened:

$$A = A' + ds_1 \quad (5)$$

where A' = measured peak amplitude, d = signal attenuation (0.75 dB mm^{-1}) and s_1 = distance to the sensor.

In our case where the attenuation is very high the fraction of acoustic emission events that can be localized is only small. Most events, however, occur under one of the sensors and cannot be localized because the distance to the other sensor is too far. Therefore we consider all non-localized events to be independent and add them without correction to the corrected data.

The stress and strain data were fed to the AET 5500 through the analogue input channels. As most of the specimen is covered with clamps and sensors, optical strain measurement cannot be used here. The strain is determined from the traverse distance. Therefore the strain data are only accurate relative to different tests but do not reflect absolute values.

4. Experimental results

4.1. Small-angle X-ray scattering

SAXS data were obtained during tensile testing of the specimens. Microcracks and voids cause scattered radiation at very high intensities due to the large difference in electron density between them and the polymer matrix. The SAXS experiments were carried out with synchrotron radiation (wavelength 0.15 nm) at HASYLAB (DESY, Hamburg) [5].

Obtaining the SAXS data was done step by step. The specimen was strained by a certain interval (strain rate 5 mm min^{-1}), e.g. $\lambda = 1.0$ to $\lambda = 1.2$ ($\lambda = l/l_0$ where l_0 = initial length); then deformation was stopped and a two-dimensional scattering image was taken by scanning with a linear position-sensitive detector. These steps were repeated several times to higher deformations.

Assuming an ellipsoid of revolution with axes a and va ($v > 1$) as the form of the microcracks, the inner part of the diffraction curve can be described in a Guinier approximation by

$$I(b) = (\Delta\rho)^2 V^2 \exp(-4\pi^2 R_d^2 b^2) \quad (6)$$

where R_d = radius of gyration, b = absolute value of the scattering vector = $2\sin\theta/\lambda$, 2θ = scattering angle,

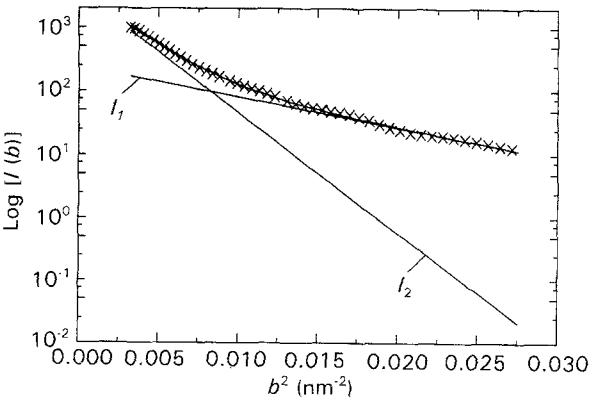

Figure 3 Guinier plot of scattering data and fitted curve: (×) experimental, (—) theoretical.

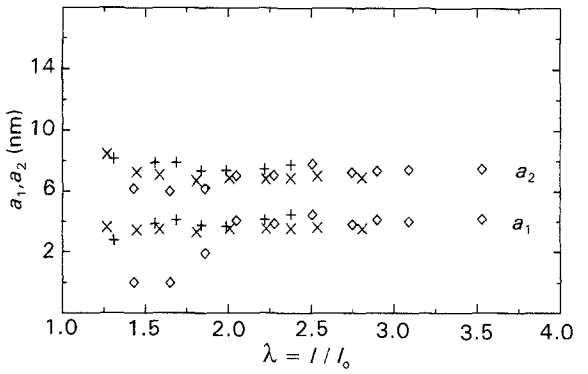

Figure 4 Results of the Guinier approximation: (×) without coupling agent, (+) with coupling agent, (◇) pure matrix.

$\Delta\rho$ = difference in electron density and V = volume of the scattering units. The diameter a of the ellipsoid is connected with the radius of gyration by $R_d = a/5^{1/2}$ [6].

It is impossible to make a statement about the large axis va, which reflects the longitudinal dimension of the microcracks parallel to the strain direction, because of limited resolution. Although the diameters of the microcracks should be distributed over a certain range, the scattering data can, to a first approximation, be described satisfactorily by a superposition of two contributions with diameters a_1 and a_2:

$$I(b) = I_{a_1}(b) + I_{a_2}(b) \quad (7)$$

Fig. 3 exemplifies the scattering data and the fitted curve together with the two contributions I_{a_1} and I_{a_2} which form a straight line in the Guinier plot (log I versus b^2). Fig. 4 shows a survey of results from fitting data sets of different specimens: the pure matrix and two composites with 20 vol% fibre addition, one with a coupling agent and the other without any coupling agent.

One can draw several conclusions from the results:

(a) The pure polymer matrix shows scattering by microcracks although it is not possible to detect any sound emission.

(b) The diameters a_1 and a_2 show no great variation during the deformation, with one difference: the pure matrix shows a slight increase in the magnitude of a_1 and a_2 during the initial phase ($\lambda < 2$). The

composites show nearly constant diameters a_1 and a_2. Obviously the formation of microcracks happens in such a short strain interval that we could not detect the initial phase. From acoustic emission analysis we found a maximum in the acoustic emission rate for composites at small strains of $\lambda \simeq 1.2$ and smaller. As soon as fibres are added to the polymer matrix, the matrix is stressed higher in the composite to get the same rate of deformation as in the specimens without any fibres. Therefore in the composite the formation of cracks should happen much earlier than in the pure matrix.

4.2. Acoustic emission during tensile testing

The rate of acoustic emission N_λ was calculated as the number of events that occur in a strain interval of $\Delta\lambda = 0.01$. In order to make diagrams from different tests comparable, the acoustic emission rate was projected to a constant strain interval of $\Delta\lambda = 0.01$. For plotting together with stress–strain curves the acoustic emission rate was multiplied with a scale factor of 10^{-2}. Fig. 5 shows the acoustic emission rate during the deformation of ETFE with 10% glass fibres without coupling agent at room temperature (20 °C).

Tensile tests were performed at different temperatures between −40 and +80 °C with a maximum strain of $\lambda \simeq 1.5$. The shapes of the stress–strain curves and the corresponding acoustic emission rate vary only slightly, but the acoustic emission rate decreases along with the yield stress. At all temperatures the composites made of fibres coated with LZ44 show less acoustic emission activity than the composites made of uncoated fibres. For comparison between different tests the average acoustic emission rate $\bar{N}_\lambda$ was calculated:

$$\bar{N}_\lambda = N/\Delta\lambda \tag{8}$$

The average acoustic emission rate $\bar{N}_\lambda$ at different temperatures is shown in Fig. 6.

4.2.1. Peak amplitude distribution

Peak amplitude distribution functions were fitted to the experimental data by the method of least squares (Fig. 7). The fixed threshold cuts off the peak amplitude distribution at a minimum value of 35 dB. Therefore the amplitude distribution function was

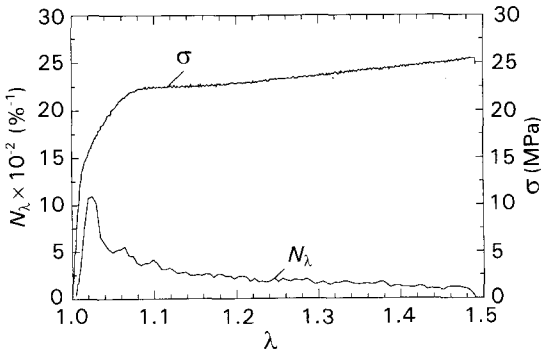

Figure 5 Acoustic emission during deformation: ETFE with 10% uncoated fibres.

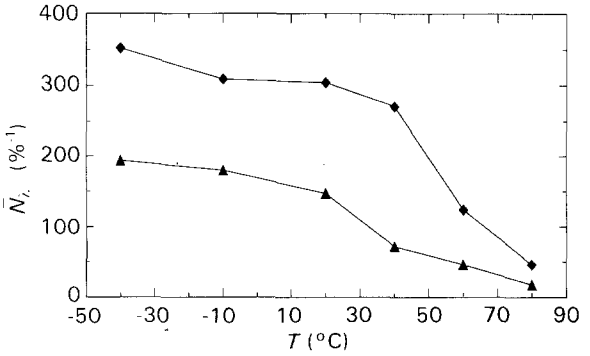

Figure 6 Change of average acoustic emission rate with temperature: ETFE with (◆) 10% uncoated fibres, (▲) 10% fibres coated with LZ44.

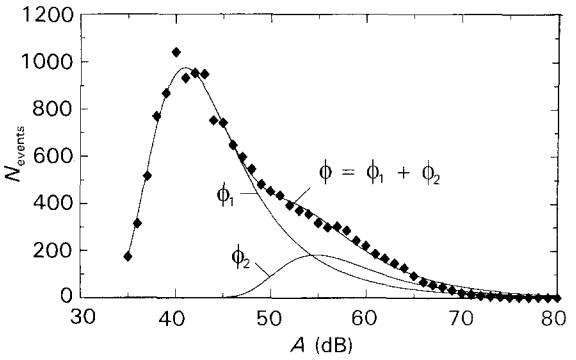

Figure 7 Peak amplitude distribution with fitted distribution function: ETFE with 10% uncoated fibres.

multiplied with a step function with a cutoff at 35 dB. The measured amplitude distributions indicate that a second failure process with a higher characteristic peak amplitude is superimposed on the main failure process. For further information about the dependence of peak amplitude on the deformation, the peak amplitude data were analysed for three different intervals of the tensile test:

(i) an interval of low strain, where the stress increases linearly and the acoustic emission is low,

(ii) the transition from linear to plastic behaviour including the yield point, where the acoustic emission reaches its maximum, and

(iii) the region of plastic flow with decreasing acoustic emission.

The fraction of events with high peak amplitude values has its maximum in the first and second interval and decreases gradually after the yield point. Fig. 8 shows as a typical example the change of the peak amplitude distribution during the deformation of ETFE with 10% glass fibres without coupling agent at room temperature (20 °C). This effect was observed in both types of composite without significant differences. The characteristic distribution function parameters (b, c) show no systematic dependence on either fibre type or temperature. Typical values for the results of fitting a peak amplitude distribution function to the experimental data are

(i) the main failure process: $b = 39.3$–41.5 dB and $c = 8.6$–10.6.

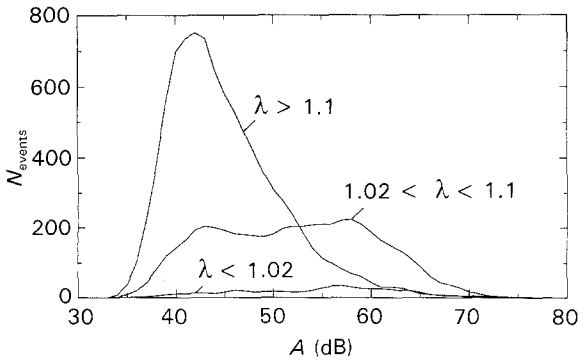

Figure 8 Change of peak amplitude distribution during deformation.

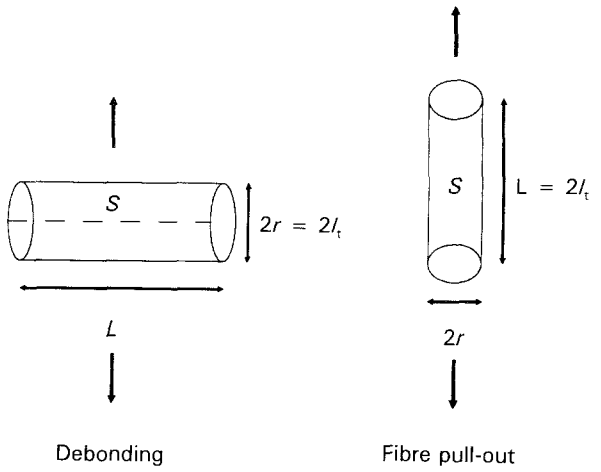

Figure 9 Model of fibre delamination processes.

(ii) a secondary failure process at low strain: $b = 51.1$–55.3 dB and $c = 9.3$–12.4.

5. Discussion

5.1. Identification of failure processes

Tests using pure matrix specimens without fibres do not show any significant acoustic emission at all. This demonstrates that acoustic emission is caused by processes related to the fibres.

Fibre breakage is only possible if the fibres are long enough. The critical fibre length l_c can be estimated by [7]

$$\frac{l_c}{d} = \frac{\sigma_f^*}{2\tau_m} \tag{9}$$

With $\sigma_m^* = 40$ MPa (yield stress of the polymer matrix), $\tau_m = 0.58\,\sigma_m^*$ (failure hypothesis of Huber, von Mises and Hencky [1]), $\sigma_f^* = 2300$ MPa (fibre strength) and $d = 10$ μm (fibre diameter) the critical fibre length is $l_c = 500$ μm. As the fibres used in the composites ($\bar{L} \simeq 60$ μm) are much shorter, fibre breakage is unlikely.

This shows that in this case acoustic emission is caused by fibre delamination processes. With respect to the results of peak amplitude distribution analysis, the main failure process was interpreted as fibre debonding. Since the fibres are oriented randomly in the specimen, failure by normal stress is the more common process. Fibre pull-out can happen only to fibres that are aligned more or less parallel to the strain direction.

5.2. Model of fibre delamination processes

Berthelot [8] suggested a one-dimensional model of microcracking in the polymer matrix. He modelled the rupture process by a mass–spring system and calculated the energy released as

$$\Delta W_u = \frac{1}{2}\left(\frac{\sigma_u^2}{E}\right) S l_t \left(1 - \frac{R}{\sigma_u S}\right)^2 \tag{10}$$

with σ_u = ultimate stress in the rupture area, E = Young's modulus of the rupture area, S = surface created during rupture, l_t = transfer length (i.e. the length of stress redistribution) and R = interaction after rupture. Neglecting the interaction after rupture R, the released energy is

$$\Delta W_u = \frac{1}{2}\left(\frac{\sigma_u^2}{E}\right) S l_t \tag{11}$$

In this case the model system was applied to fibre delamination processes. We consider two different processes representing the extreme cases that can occur (Fig. 9).

(i) Fibres with orientation perpendicular to the strain direction undergo debonding because of stress normal to the fibre surface. The debonding process is considered to be constrained to one side of the fibre. With $l_t = r$ and $S = \pi \bar{L} r$ where $\bar{L}$ = mean fibre length, the energy released by fibre debonding is

$$\Delta W_{debonding} = \frac{1}{2}\left(\frac{\sigma_m^2}{E}\right) \pi \bar{L} r^2 \tag{12}$$

(ii) Fibres with their axis oriented parallel to the strain direction are pulled out of the matrix because of shear stress. The transfer length representing the range of stress redistribution is estimated as $l_t = \bar{L}/2$, the decohesion surface is the fibre surface $S = 2\pi r \bar{L}$, and following von Mises [1] the maximum shear stress was estimated as $\tau_m = 0.58\,\sigma_m$. Then

$$\Delta W_{pullout} = \frac{1}{2}\left(\frac{\tau_m^2}{E}\right) \pi r \bar{L}^2 \tag{13}$$

This simple calculation shows that in general fibre pull-out releases more energy than fibre debonding. Since the peak amplitude of an acoustic emission event is proportional to the energy of the underlying failure process, the expected difference in peak amplitude between the two extreme processes is

$$\Delta A = 20 \log\left(\frac{\Delta W_{pullout}}{\Delta W_{debonding}}\right) \tag{14}$$

$$= 20 \log(0.67 v) \tag{15}$$

with $v = \bar{L}/2r$. In this case ($v \simeq 5$) the expected difference in peak amplitude is $\Delta A \simeq 10.5$ dB. Considering that this simple model does not take into account the effects of coupling agents and interactions between adjacent fibres, the calculation agrees well with our results.

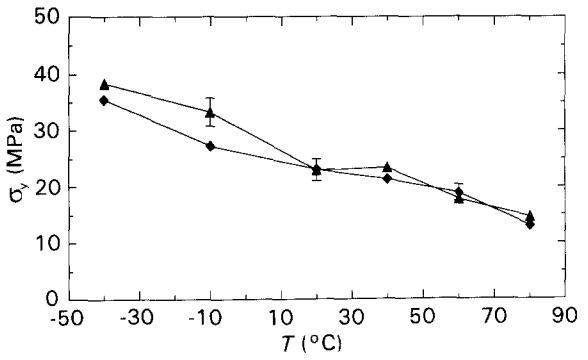

Figure 10 Change of yield stress with temperature: ETFE with (◆) 10% uncoated fibres, (▲) 10% fibres with LZ44.

5.3. Influence of temperature and coupling agent

Fig. 10 shows that, especially at low temperatures, the coupling agent increases the yield stress of the composite. With increasing testing temperature the acoustic emission decreases along with the mechanical yield stress. The polymer matrix becomes more ductile and fibre delamination processes are reduced because the stress transfer to the fibres decreases. Also the composites with fibres coated with coupling agent show less acoustic emission due to better fibre–matrix adhesion. The energy released by fibre delamination, however, which is related to the peak amplitude of the acoustic emission signal, does not depend significantly on temperature or fibre coating. According to the model calculations the decrease in matrix strength at high temperature and the improved fibre–matrix adhesion by the coupling agent should reduce the peak amplitude of acoustic emission events; this was not observed. It may be that the stress transfer length and the fracture surface rise with decreasing matrix strength, and level off the influence on the characteristic peak amplitude. Probably these effects are too small to exceed the statistical variation of the fitted parameters. Further SAXS and acoustic emission experiments are planned for getting more information about this point.

Acknowledgements

We are grateful for the support of the Deutsche Forschungsgemeinschaft (DFG) and the BMFT. The experiments with synchrotron radiation were funded by the German Federal Ministry for Research and Technology (BMFT) under contract No. 05479AAB. For the supply of specimen materials we thank the Hoechst AG, Gendorf.

References

1. J. WOLTERS, "Anwendung der Schallemissions-Messtechnik zum Beschreiben von Versagensmechanismen in partikelgefüllten Thermoplasten", Fortschr.-Ber. VDI Reihe 5 Nr. 163 (VDI, Düsseldorf, 1989).
2. R. A. KLINE and S. S. ALI, *J. Acoust. Emission* **4** (1985) 107.
3. L. LORENZO and H. T. HAHN, *ibid.* **5** (1986) 15.
4. Y. H. WU, M. H. YANG, J. Y. KUO and S. P. CHANG, in Proceedings of SPI International Symposium on Acoustic Emission from Reinforced Composites, Montreal, 1986, Vol. 2, p. 37.
5. R. GEHRKE, *Topics Curr. Chem.* **151** (1989) 111.
6. A. GUINIER, "X-ray Diffraction in Crystals, Imperfect crystals and Amorphous Bodies" (Freeman, San Francisco, 1963) p. 328.
7. A. A. BERLIN, S. A. VOLFSON, N. S. ENIKOLOPIAN and S. S. NEGMATOV, "Principles of Polymer Composites" (Springer, Berlin, 1986) p. 6.
8. J. M. BERTHELOT, *J. Reinf. Plast. Compos.* **7**(3) (1988) 284.

Received 18 February
and accepted 10 December 1992